Interchangeable biomass fuels for paper-based microfluidic fuel cells: finding their power densities limits

André L. D. Lima,[ab] Piter M. Rocha,[a] Adilson C. Silva,[b] Jesum Alves Fernandes,[c] Cauê A. Martins*[ac]

[a]Electrochemistry Research Group, Institute of Physics, Federal University of Mato Grosso do Sul, Campo Grande 79070-900, Brazil

[b]Department of Chemistry, Institute of Exact and Biological Sciences, Federal University of Ouro Preto, Ouro Preto 35400-000, Brazil

[c]School of Chemistry, University of Nottingham, Nottingham NG7 2RD, United Kingdom

*caue.martins@ufms.br

ABSTRACT: Paper batteries are self-pumping emerging tools for powering portable analytical systems. These disposable energy converters must be low-cost and must achieve enough energy to power electronic devices. The drawback is to reach high energy keeping the low cost. Here, for the first time, we report a paper-based microfluidic fuel cell (PµFC) equipped with Pt/C on carbon paper (CP) anode and a metal-free CP cathode fed by biomass-derived fuels to deliver high power. The cells were engineered in mixed media configuration, where methanol, ethanol, ethylene glycol, or glycerol is electro-oxidized in an alkaline medium while $Na_2S_2O_8$ is reduced in an acidic medium. This strategy allows for optimizing each half-cell reaction independently. The colaminar channel of the cellulose paper was chemically investigated by mapping the composition, which reveals a majority of elements from the catholyte and anolyte on each respective side, and a mixture of both at the interface, assuring the existing colaminar system. Moreover, the colaminar flow was investigated by investigating the flow rate considering recorded videos for the first time. All PµFC shows 150-200 s to build the stable colaminar flow, which matches the time to reach a stable open circuit voltage. The flow rate is similar for different concentrations of methanol and ethanol, but it decreases with the increase in ethylene glycol and glycerol concentrations, suggesting longer residence time for the reactants. The cells perform differently for the different concentrations, and their limiting power densities are composed of a balance among anode poisoning, residence time, and viscosity of the liquids. The sustainable PµFCs can be interchangeably fed by the four biomass-derived fuels to deliver ~2.2-3.9 mW cm⁻². This allows choosing the proper fuel due to their availability. The unprecedented PµFC fed by ethylene glycol delivered 6.76 mW cm⁻², which is the benchmark output power for a paper battery fed by alcohol.

Keywords: Paper batteries; Metal-free cathode; Methanol; Ethanol; Ethylene glycol; Glycerol.

1. Introduction

The impending need to transit towards sustainable and clean energy has opened new promising research fields regarding the development of alternative energy supplies. Microfluidic fuel cells (µFCs) appear as potential energy converters to power small devices[1] and even conventional electric machines whether properly scaled out.[2] The working principles of µFC are similar to those of fuel cells, where fuel is oxidized at the anode, and an oxidant is reduced at the cathode while the electrons flow through an external circuit. The difference is that conventional fuel cells use an ionic permeable membrane while µFCs use colaminar flow to allow internal ion transport to close the circuit.[1-3] This is achieved by engineering the microchannel to allow laminar flow at a low Reynold's number in the micrometer scale.[2] The absence of a membrane excludes the ohmic drop and price intrinsically related to such a component.[3] Since there is no membrane, each half-cell reaction can be independently optimized to its best configuration,[4] such as electrooxidation in an alkaline medium and reduction in an acidic medium, called mixed-media configuration.[2]

The mixed-media configuration allied to the use of porous electrodes in flow-through configuration[5] has been used to boost the output power of µFC fed by biomass-derived alcohols.[6-10] Methanol, ethylene-glycol, ethanol, and glycerol have been investigated as potential fuels,

theoretically producing 6, 10, 12, and 14 electrons per molecule completely oxidized, respectively.[2] Although the cleavage of the C-C bonds of ethanol, ethylene glycol, and glycerol makes it difficult to convert it into CO_2 (CO_3^{2-} in alkaline medium) on planar electrodes;[11–13] the flow-through configuration increases reactants usage, increasing the efficiency of conversion.[9,10]

The biomass-fed μFCs made of PDMS[8,14] and 3D-printed[7] reached hundreds of mW cm^{-2} and may be further scaled out. These devices require an external pump to conduct the flow of the liquids through the Tygon tubes, which is an additional negative contribution in terms of energy for the miniaturized device. Moreover, building PDMS cells requires well-trained operators and special instrumentation,[15] and although the 3D-printed cell has arisen as an important alternative for manufacturing,[7] the understanding of the laminar flow on the printed pieces is still unknown and may face challenges in reproducibility. In this context, paper-based microfluidic fuel cells (PμFCs) may overcome these drawbacks.

The capillary forces move the flow through the porous of the cellulose papers. Hence, PμFCs are self-pumping systems, excluding the need for external forces and additional energy, accordingly.[16] Besides, capillarity is an intrinsic feature of the paper, making it extremely reproducible.[16,17] Tanveer et al. schematically reviewed the historical development and state-of-the-art PμFCs.[16] The use of paper to pump the flow gathers advantages such as low-cost, lightweight, flexibility, biodegradability, portability, scalability, and reproducibility.[16,18] Thus, building PμFCs fed by biomass-derived fuels seems a good strategy to aggregate value to these clean and renewable alcohols.

At least to our knowledge, there are few papers regarding the PμFCs fed by methanol and ethanol,[19–21] and we could not find PμFCs fed by ethylene glycol or glycerol in the literature. Ethylene glycol is a widely available alcohol that can be obtained from sugars via microorganisms. Glycerol is a 10% byproduct of biodiesel fabrication with a very low market price and high theoretical energy density.[22] Thus it is worth the effort in investigating these alcohols as fuels. Regarding the use of methanol, Esquivel et al. developed a device equipped with PtRu particles on Au/COP anode and a Pt on carbon paper (CP) cathode placed on a self-pumping paper capable of delivering 1-5 mW cm^{-2}.[19] Regarding ethanol usage, Chandra et al. built an ethanol/dichromate PμFC equipped with molybdenum oxide nanorods as anode and cathode, producing 6.32 mW cm^{-2} of maximum power density.[20] Rao et al. also investigated PμFC fed by ethanol with different experimental configurations and catalysts to achieve ~0.072 mW cm^{-2}.[21] It is clear that this research field is promising and unexplored and demands improvement to fit the requirements for practical applications.

Therefore, here we built PμFCs fed by exchangeable biomass-derived alcohols. The cells operate with the anodic reaction in an alkaline medium on the Pt/C on carbon paper (CP) while sodium persulfate in an acidic medium is reduced on a metal-free CP cathode. Namely, we feed the PμFCs with different concentrations of methanol, ethylene glycol, ethanol, and glycerol to find their limit output power. The concentration of the fuels can be controlled to produce a similar output power density at around 2-4 mW cm^{-2} considering their concentration. The power density can be boosted to 6.76 mW cm^{-2} using ethylene glycol, which is the benchmark for a PμFC fed by alcohol. The limit power densities are composed of a balance among anode poisoning, capillarity and residence time, and viscosity of the liquids.

2. Experimental

2.1. Half-cell reactions and materials characterization

Before building the PμFC, each reaction was studied in half-cell measurements. Strips of carbon paper Toray® TGP-060 were left in 2 mL plastic containers filled with 10 mg of 5 nm Pt/C (60%, E-TEK®) dispersed in 900 μL water + 900 μL methanol + 200 μL Nafion® 5%, which is the catalytic ink to prepare the anode. Then, the pieces were dried in an oven at 80 °C for 4 h. The Pt/C/CP electrodes are cut into 10 x 5 mm to be used as working electrodes. For these experiments, ~6 mm of the Pt/C/CP is immersed in the solution, a high-area Pt plate is used as a counter electrode, and an Ag/AgCl as a reference electrode. The Pt/C/CP was held by a toothless crocodile for electric contact. Using a Potentiostat/Galvanostat PalmSens3, the Pt/C/CP electrodes were investigated in 1.0 mol L^{-1} KOH and O_2-free solution of methanol, ethanol, ethylene glycol, or glycerol in different concentrations by cyclic voltammetry between -1.0 and 0.5 V. The currents were normalized by the electrochemically active surface area considering 210 μC cm^{-2} as the charge involved in the desorption of a hydrogen monolayer on platinum. The reduction of 0.5 mol L^{-1} $Na_2S_2O_8$ in 1.0 mol L^{-1} H_2SO_4.was investigated on a metal-free CP between 1.6 and 0.2 V. All measurements were performed at 0.05 V s^{-1}.

The modified and unmodified carbon paper and the cellulose paper were studied by scanning electron microscopy images in an SEM JEOL model JSM-6380LV. The chemical composition was studied by coupling the SEM to an energy-dispersive X-ray detector (EDX) Thermo Scientific (model Noran System Six). The cellulose paper was characterized before and after use on both sides of the colaminar flow. **Figure S1** shows illustrative images of CP and Pt/C/CP with their respective EDS spectra.

2.2. Fuel cell tests

After acquiring electrocatalytic parameters from the half-cell measurements, we performed fuel cell tests by collecting polarization and power density curves. The PμFCs were built in a colaminar flow configuration, as illustrated in **Figure 1**. The fuel cell was placed and slightly pressed on a 5.1 x 4.6 cm plastic plate printed in a SethiS3 3D printer using polyethylene terephthalate glycol filament (PETG) (**Figure S2**). The inlets of liquids are 6 mm long independent channels immersed in catholyte and anolyte. The liquids flow through the paper, building a 1 x 5 mm colaminar channel between the electrodes and towards a paper pad adsorbent, shown in the inset of **Figure 1**. The CP cathode

and the Pt/C/CP anode are placed on the colaminar flow to form a flow-over configuration. Both electrodes were cut into 5 x 6 mm. The cathode could also be considered air-breathing, but the oxygen reduction reaction is almost inconsiderable compared to the reduction of the liquid oxidant. The PµFC was designed in a simple and well-known architecture, aiming to investigate the use of biomass-derived fuels as the sole variable. A similar design can be found elsewhere,[18] and the mechanism of fluid transporting throughout the paper is based on the capillarity of the cellulose paper, without intricated sets of hydrophilic/hydrophobic patterns.[23]

The polarization curves were collected by linear voltammetry from the OCV to 0.001 V at 0.01 V s^{-1}. The power density curves were built by multiplying the current density by the cell voltage. The measurements were performed from 0.05 to 2.5 mol L^{-1}, depending on the alcohol, as discussed later, keeping the catholyte constant as 0.5 mol L^{-1} Na$_2$S$_2$O$_8$ in 1.0 mol L^{-1} H$_2$SO$_4$. All measurements were performed in triplicate. Worth noting that CP is 190 µm thick, forming a 0.011 cm^2 cross-sectional area, which is used to normalize current and power. A real photo of the PµFC is shown in **Figure S2**.

We also monitored the flow rate of the liquids in cm s^{-1}. We considered the variation of a one-dimension line in front of a wave (*dl*) as a function of time (*dt*) for the colaminar channel to calculate the velocity of the flow or flow rate. The measurements were made from print screens of recorded videos – detailed in due course. This strategy was used to avoid weighting the paper to collect the difference in mass and further the difference in volume, which is usually done to report rates in mL min^{-1}. We suggest the current method (cm s^{-1}) because of its accuracy. Since we used the same cellulose filter paper (Qualy®) for all measurements, we focused on identifying the influence of the solution on the velocity of the flow, which is achieved by the *dl/dt* plots.
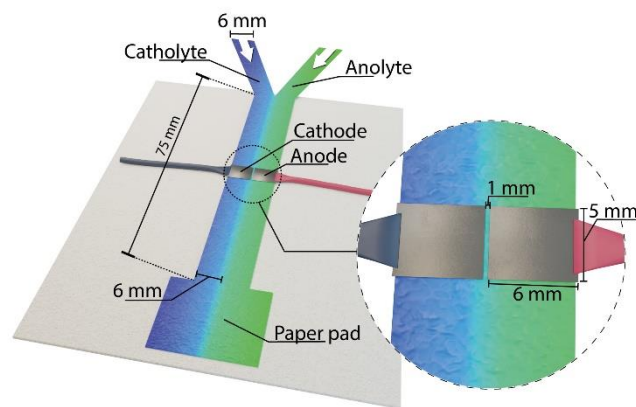
Figure 1. Illustration of the paper-based mixed-media microfluidic fuel cells fed by biomass-derived alcohols and sodium persulfate in colaminar and flow-over configuration. The inset shows the colaminar channel.

3. Results

The complete electrooxidation of the biomass-derived alcohols leads to CO$_2$, as shown in equations 1-4. However, CO$_2$ is chemically converted to carbonate in an alkaline medium, as shown in equation 5, which avoids micro bubbles disturbing the laminar flow and keeps the carbon *remanded* instead of releasing it to the environment. Besides, the use of oxygen as an oxidant may lead to the cathodic reaction into H$_2$O, which dilutes the catholyte,[16] decreasing the efficiency of the half-cell reaction that has lower kinetics, and the overall reaction accordingly. Here we use a liquid oxidant sodium persulfate to form an anion as a product, as shown in equation 6. Therefore, considering these advantages in further application, we performed the half-cell reactions.

$$CH_3(OH) + 6OH^- \rightarrow CO_2 + 5H_2O + 6e^- \qquad \text{eq. 1}$$
$$C_2H_5(OH) + 12\,OH^- \rightarrow CO_2 + 9H_2O + 12e^- \qquad \text{eq. 2}$$
$$C_2H_4(OH) + 10OH^- \rightarrow 2CO_2 + 18H_2O + 10e^- \qquad \text{eq. 3}$$
$$C_3H_5(OH) + 14OH^- \rightarrow 3CO_2 + 11H2O + 14e^- \qquad \text{eq. 4}$$
$$CO_2 + 2OH^- \rightarrow CO_3^{2-} + H2O \qquad \text{eq. 5}$$
$$S_2O_8^{2-} + 2e^- \rightarrow 2SO_4^{2-} \qquad \text{eq. 6}$$
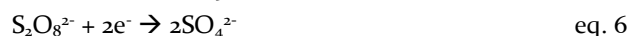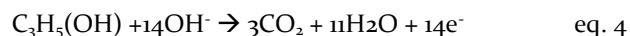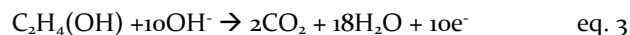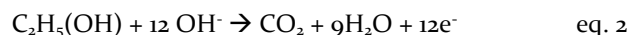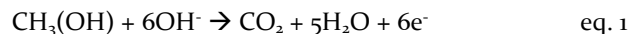
3.1. *Half-cell investigation*

The fundamental experiments performed in a conventional three-electrodes cell provide important thermodynamics information in terms of onset potential and kinetics, such as current density. **Figure 2** shows the cyclic voltammograms of the biomass-derived alcohols on Pt/C/CP in an alkaline medium. These results are part of a few reports in the literature,[8,14,24] showing half-cell measurements of the porous electrodes instead of the response of nanoparticles deposited on a smooth surface. This analysis is important because considers the capacitive current of the CP, besides its resistivity in aqueous solutions.

The voltammograms are characteristic of small-chain-alcohols, with anodic current on both forward and backward scans, as shown in **Figure 2**. The concentrations of the alcohols are indicated in the figure, being from 0.05 to 1.0 mol L^{-1} for all fuels, and with higher concentrations for ethylene glycol and glycerol to elucidate the influence on the power density, as discussed later. In general, there is a wide anodic peak towards positive potential, followed by an inactivation due to the formation of the oxide; and a surface reactivation after the reduction of such oxides at the negative scan, leaving free-active sites to oxidize the alcohols. The reduction of surface oxides is more evident in 0.05 mol L^{-1} for all alcohols, with a cathodic peak at ~-0.3 V.

The most important parameters investigated here are the onset potential (E$_{onset}$), current density, and the influence of the concentration on the output current. The E$_{onset}$ is ~-0.6 V for methanol electrooxidation on Pt/C/CP (**Figure 2A**), while the potential peaks displaced toward more positive values with the increase in concentration. The current density increases with methanol concentration up to 1.7 A cm^{-2} in 1.0 mol L^{-1} (**Figure 2A**). Similar behavior is shown for ethanol electrooxidation (**Figure 2B**). The E$_{onset}$

is lower than that for methanol, at ~-0.67 V. The current also increases with concentration from 0.05 to 0.5 mol L^{-1} but is slightly lower for 1.0 mol L^{-1}.

The ethylene glycol electrooxidation starts at ~-0.55 V and shows higher current densities than that found for the other fuels (**Figure 2C**). The current density is 2.2 A cm^{-2} for 0.05 mol L^{-1} and reaches ~22.7 A cm^{-2} for 2.0-2.5 mol L^{-1}. Thus, it is clear that the two hydrated carbons with only one bond are more easily oxidized than the other alcohols. Using the same catalyst and 1.0 mol L^{-1} of the fuel, the output current density for such a reaction (17.5 A cm^{-2}) is ~10, ~19, and ~9 fold those found for methanol, ethanol, and glycerol, respectively.

Glycerol electrooxidation reaction on Pt is even more complex,[13,13,25,26] and the current density increases until a maximum, when the surface poisoning caused by partially oxidized compounds and CO are deleterious.[27] The E_{onset} of glycerol electrooxidation on Pt/C/CP is at ~-0.57 V for all concentrations, while the current density increases from

0.05 to 1.0 mol L^{-1} and decreases for 1.5 mol L^{-1} (**Figure 2D**). The maximum current density was 1.9 A cm^{-2} for 1.0 mol L^{-1}.

The concentration plays an important role in the poisoning of the Pt surface,[10,28] and sometimes adjusting the correct concentration improves more the reaction than when using a new advanced material. Thus, here we explore the influence of concentration on the performance of the PµFCs. All anodic reactions show similar E_{onset} at around -0.55 to -0.60 V. Considering that the E_{onset} for the cathodic reaction is 0.49 V (**Figure S3**), the OCV is expected to be ideally at around 1.0 V. Most importantly, coupling the biomass-derived electrooxidation in alkaline medium with Na$_2$S$_2$O$_8$ reduction in acidic medium promotes negative free-Gibbs energy for the overall reaction, allowing us to use this configuration to produce power. Before investigating the output power, we characterized the system itself.
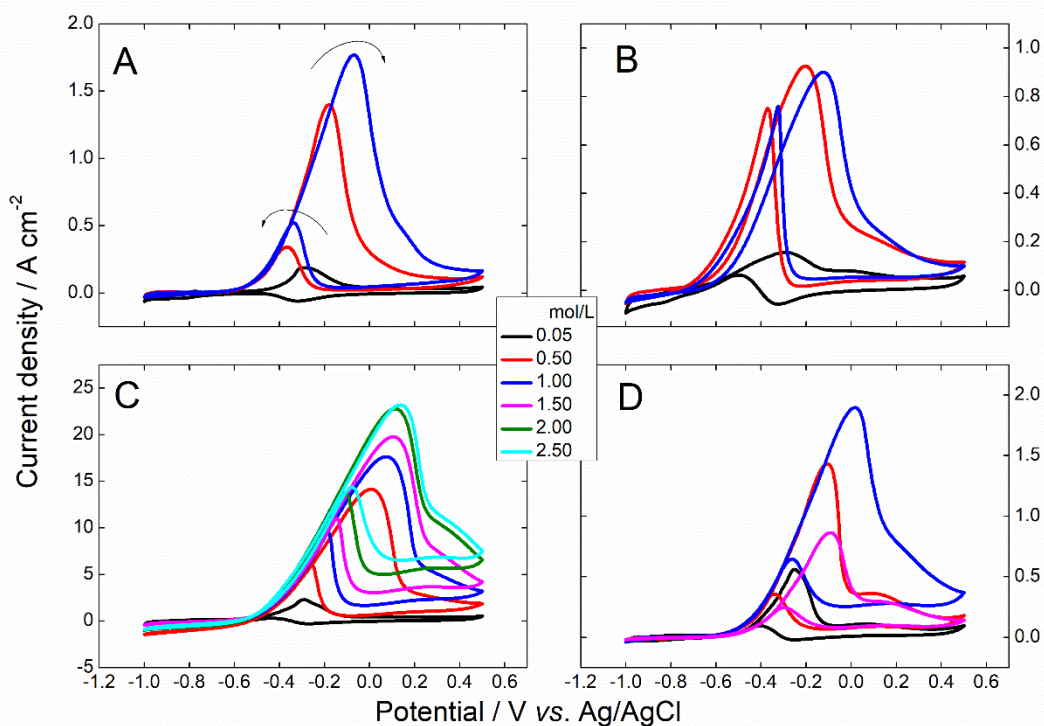
Figure 2. Fifth cyclic voltammogram of Pt/C/CP in (A) methanol, (B) ethanol, (C) ethylene glycol, and (D) glycerol in 1 mol L^{-1} KOH at 0.05 V s^{-1}. Concentrations are indicated in the Figure.

3.2. *Characterizing the paper and the flow*

Before the fuel cell tests, the colaminar flow formation was microscopically investigated by flowing a model anolyte, 1 mol L^{-1} methanol in 1 mol L^{-1} KOH, and 0.5 mol L^{-1} Na$_2$S$_2$O$_8$ in 1.0 mol L^{-1} H$_2$SO$_4$ as catholyte. The micrographs and EDS spectra of a model of the PµFCs are shown in **Figures 3A-3H**. The micrographs of both sides of the paper fuel cell are similar, without physical discrepancies, shown in **Figures 3A** and **3C** for the cathode and anode sides respectively. The EDS of the cellulose paper before use shows mainly the presence of carbon and oxygen (**Figure 3B**).

After flowing the catholyte and anolyte in a model of the PµFC (**Figure 3E**), the chemical composition of the paper becomes different from side to side. It is worth noticing that this is an *ex-situ* investigation, thus the paper is dried before the SEM measurements, which induces a mixture of reactants until total drying. The catholyte side shows a strong signal of S, K, and Na (**Figure 3D**). The S and Na come from the catholyte itself, Na$_2$S$_2$O$_8$ in H$_2$SO$_4$, while the presence of K is due to the capillary movement of the anolyte during the drying. Note that the signal of S (from catholyte) is more intense than that of K (originally from

anolyte). **Figure 3F** shows the EDS spectrum of the anolyte side after drying. The signal from K (from anolyte) is more intense than that from S (originally from catholyte). The peak from Na is almost unseen. Thus, besides the expected mixture during drying, it is evident that each side still conservates the expected major composition of the respective liquids that went through.

Now looking at the region where the colaminar flow is built (**Figure 3E**), we found a different composition after drying. **Figure 3G** shows a mapping chemical composition of the colaminar region highlighting the main compounds, Na, S, and K, all overlapped. The EDS spectrum of this region reveals more equivalent intensities of the peaks related to S and K from catholyte and anolyte, respectively (**Figure 3H**). Therefore, using the elements as probes, the results assure that the colaminar flow was properly built and that the system can be used to convert energy in fuel cell configuration.

Besides the chemical composition of the colaminar channel, we characterized the flow rate of the biomass-derived fuels throughout the cellulose paper. Convective mass transport takes place by partition, where the solubility of the compounds of the electrolytes in adsorbed water from the cellulose paper plays an important role. Therefore, capillarity is the main driven force for the flow.[29] The two self-pumped paths drive the flow through the paper towards the main channel and eventually to the paper pad, all by capillarity. Since the cellulose paper is the same in all measurements, the viscosity of the solution may impact the mass transfer. Therefore, following the flow rate is a way of investigating these two coupled behaviors, indirectly revealing the residence time of the reactants. Here we showed the influence of fuel concentration on the capillarity for the first, rationalized as flow rate in terms of cm s^{-1}.
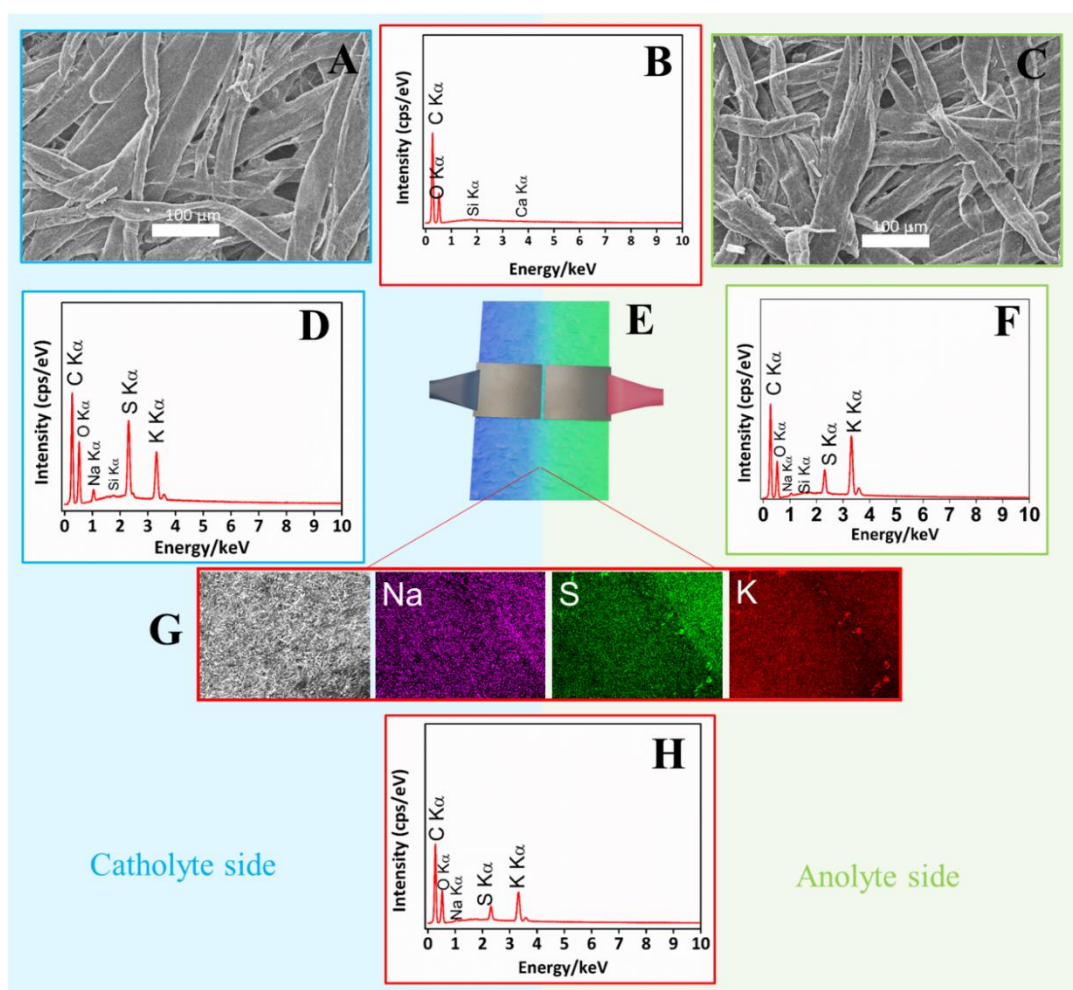
Figure 3. Micrograph characterization of the PµFC. Features (A) SEM image of the catholyte side, (B) an EDS spectrum of the cellulose paper before use, (C) SEM image of the anolyte side, (D) EDS spectrum of the catholyte side, (E) an illustrative model of the PµFC, (F) EDS spectrum of the anolyte side, (G) chemical mapping composition and (H) EDS spectrum of the colaminar region. All measurements were performed after spontaneously drying the paper. The sample was prepared by flowing a model anolyte, 1 mol L^{-1} methanol in 1 mol L^{-1} KOH, and by 0.5 mol L^{-1} Na$_2$S$_2$O$_8$ in 1.0 mol L^{-1} H$_2$SO$_4$ as catholyte.

Figure 4 shows curves of distance *vs*. time for measurements with fixed catholyte and anolytes with different fuel concentrations. All flow rates were calculated from print screens from a recorded video, as shown in the illustrative PµFC model in **Figure S4**, detailing the method.

The choice for the concentrations is based on their limiting power densities, further discussed. The curves display an apparent logarithmic growth, with a great inclination up to ~150-200 s, which we conjecture is the lapse time taken from the front of a wave to stabilize the colaminar channel, overlapping with the time waited to stabilize the OCV, highlighted in yellow backgrounds in **Figure 4**. From that point onwards, the curves show some linearity.

Different methanol concentrations change the rate that the stable colaminar channel is achieved, being faster for 0.05 and 0.5 mol L^{-1}, as shown by the inclinations of the curves (yellow background in **Figure 4A**). After that point, the flow rate does not change with concentration since the derivative of the linear part is approximately the same. **Figure S5A** shows overlapped linear fittings. The flow rates range around 5.40-4.5 10^{-3} cm s^{-1} (**Table S1**). This suggests that neither the solubility of the anolyte with methanol in adsorbed water from cellulose paper is affected nor the viscosity interferes greatly. We found similar behavior for PµFC fed by ethanol. The time to reach a stable colaminar channel is similar for 0.05, 0.5, and 1.0 mol L^{-1} (**Figure 4B** and **Figure S5B**). In the linear part, the changes in flow rates are negligible (~5.00-4.00 10^{-3} cm s^{-1} in **Tables S1**).

It is expected that different concentrations of more viscous fuels impact the flow rates. 0.05 and 0.5 mol L^{-1} of ethylene glycol display similar behavior in the whole range of time (**Figure 4C** and **Figure S5C**). The time-lapse to stabilize the colaminar channel starts to change with 1.5 mol L^{-1} and it is delayed for 2.0 and 2.5 mol L^{-1} (yellow background in **Figure 4C**). The flow rates found in the linear part decrease with the increase in concentration, which is evidenced by the linear fittings in **Figure S5C**. The flow rates are more affected by ethylene glycol concentration than by methanol and ethanol. The flow rate is ~7.7 10^{-3} cm s^{-1} for 0.05 and 0.5 mol L^{-1} and decreases up to 3.23 10^{-3} cm s^{-1} for 2.5 mol L^{-1} ethylene glycol (**Table S1**).

Although soluble in water, glycerol is more viscous than ethylene glycol, and the trends in capillarity for the different concentrations are not as obvious (**Figure 4D**). The changes in time to reach the stable colaminar flow are negligible. The inclinations are similar between 0.05 and 0.5 mol L^{-1} and are smaller for 1.0 mol L^{-1}, which is similar to that for 1.5 mol L^{-1} (**Figure 4D** and **Figure S5D**). Interestingly, the curves are roughly linear after 200 s for PµFCs fed by 0.05 and 0.5 mol L^{-1}; however, there is a second inclination after ~700 s for cells fed 1.0 and 1.5 mol L^{-1}, indicating a decrease in flow rate (**Figure 4D**). The flow rates are ~7.0 and 7.7 10^{-3} cm s^{-1} for 0.05 and 0.5 mol L^{-1} of glycerol, respectively, but drop to ~half for 1.0 and 1.5 mol L^{-1} (**Table S1**). The trend in flow rates for each alcohol is found in **Figure S6**. The change in concentration affects more ethylene glycol and glycerol than methanol and ethanol due to their higher initial viscosities, while methanol and ethanol are less viscous even pure. In general, the residence time of the reactants is virtually the same for cells fed by methanol and ethanol regardless of the concentration, and it increases with the increase in concentrations of ethylene glycol and glycerol, which may impact the overall efficiency of the systems.

It is important to note that the flow rate of a fully wetted paper (Q) depends on the dynamic viscosity (μ) by Darcy's law,[30,31] as follows,

$$Q = \frac{\kappa A \Delta P}{\mu L}$$

where κ is paper permeability, A the cross-sectional area, ΔP is the pressure difference, and L is the distance traveled by the fluid front. Therefore, the higher the viscosity, the lower the flow rate, inducing longer residence times. The dependence of flow rate with μ is less obvious for the diluted solutions when the water solvent is dominant. Analyzing the same fuel, the more concentrated solution is expected to show a lower flow rate, and longer residence time – see velocities for cells fed by ethylene glycol in **Table S1.**
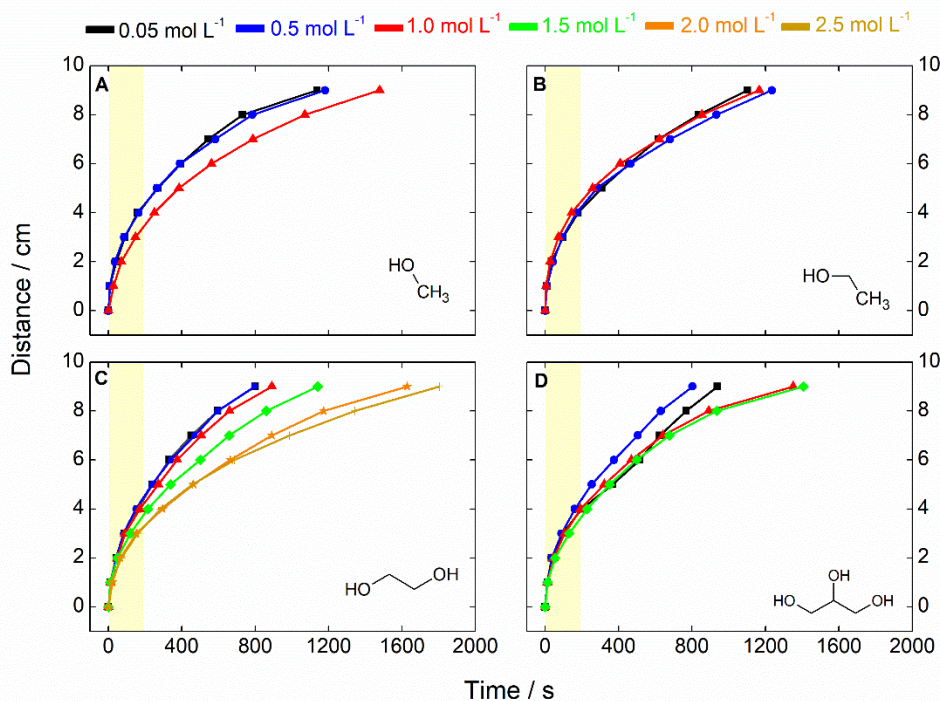
Figure 4. Distance *vs*. time for PμFCs fed by (A) methanol, (B) ethanol, (C) ethylene glycol, and (D) glycerol in 1 mol L^{-1} KOH anolytes and by 0.5 mol L^{-1} Na$_2$S$_2$O$_8$ in 1.0 mol L^{-1} H$_2$SO$_4$. Concentrations are indicated in the Figure. The light yellow background marks the range from 0 to 200 seconds.

3.3. *Fuel cell experiments*

The performance of the mixed-media PμFCs fed by the biomass alcohols in different concentrations is rationalized in terms of polarization (cell voltage *vs*. current density) and power density curves (power density *vs*. current density), as shown in **Figure 5** and **Figure S7**. The average feature of the polarization curves is similar for all systems. There is a prominent activation polarization at low current densities, which is due to the flow-over configuration of the electrodes, decreasing the collision factor for the anodic reaction allied to the well-known poisoning of Pt by CO that occurs for all four alcohols' electrooxidation.[10,12,26] The curves are mostly controlled by ohmic polarization, indicated by the monotonous decay in cell voltage at most of the current density range. Finally, the maximum current density obtained close to the short circuit is different from a profile of a limiting current found in polarization by starvation, when the oxidant is faster consumed than the rate of electrons coming from the anode side. This suggests that the catholyte with liquid oxidant is feeding the cell at enough rate to collect the electrons harvested by the anode.

The PμFCs fed by methanol display the lowest currents and power densities among the cells (**Figure 5A**). The cell operating with 0.05 mol L^{-1} methanol displays negligible response, the performance improves for 0.5 mol L^{-1} and decreases for 0.5 mol L^{-1}, achieving the best performance as 2.8 mW cm^{-2}. This is not far from the state-of-the-art power density for a PμFC fed by methanol (~5 mW cm^{-2})[19], and we used a metal-free cathode here. The power density

decreases when feeding the cell with 1.0 mol L^{-1} methanol, which could be due to a deleterious competition between increasing the amount of fuel and CO poisoning. Similar characteristics are found for the maximum current density, which reaches 28.6 mA cm^{-2} at 0.05 mol L^{-1}. The performance parameters are detailed in **Table 1**. The flow rates are virtually similar for the different concentrations (**Table S1** and **Figure S6**), thus the residence time has negligible impact on the performance.

The use of ethanol as fuel improves the overall performance of the PμFC (**Figure 5B**). The OCV for cells fed by 0.5 and 1.0 mol L^{-1} displays similar values to those for methanol, at around 0.20 and 0.25 V. The power density is also negligible at 0.05 mol L^{-1}, increases at 0.5 mol L^{-1}, and decreases at 1.0 mol L^{-1}. However, the peak power density values are different. The flow rates are similar for the three concentrations, thus the influence of residence time is negligible compared to the impact of the surface reaction (**Table S1** and **Figure S6**), suggesting that at 1.0 mol L^{-1}, the amount of fuel leads to intense CO poisoning, compromising the adsorption of ethanol, which is deleterious for the cell.

The PμFC fed by ethanol reached 3.7 mW cm^{-2} and 60.8 mA cm^{-2} at 0.5 mol L^{-1}. This evidences that besides the CO poisoning and the possible formation of acetic acid,[32] ethanol can be a good choice because is a less toxic and more promising fuel than methanol. More details are found in **Table 1**. This value is an order of magnitude higher than that found using stacked cells and multi-walled carbon nanotubes in buckypaper as electrodes.[21] This output

power is higher than that found for a PµFC fed by ethanol and dichromate (2.74 mW cm⁻²)[20], and lower compared to the same system when equipped with molybdenum oxide nanorods as catalysts (6.32 mW cm⁻²).[20] Therefore, the ethanol PµFC proposed here adds advantages since it delivers high power using a nontoxic liquid oxidant, metal-free cathode, and easily found commercial Pt/C NPs at the anode side.
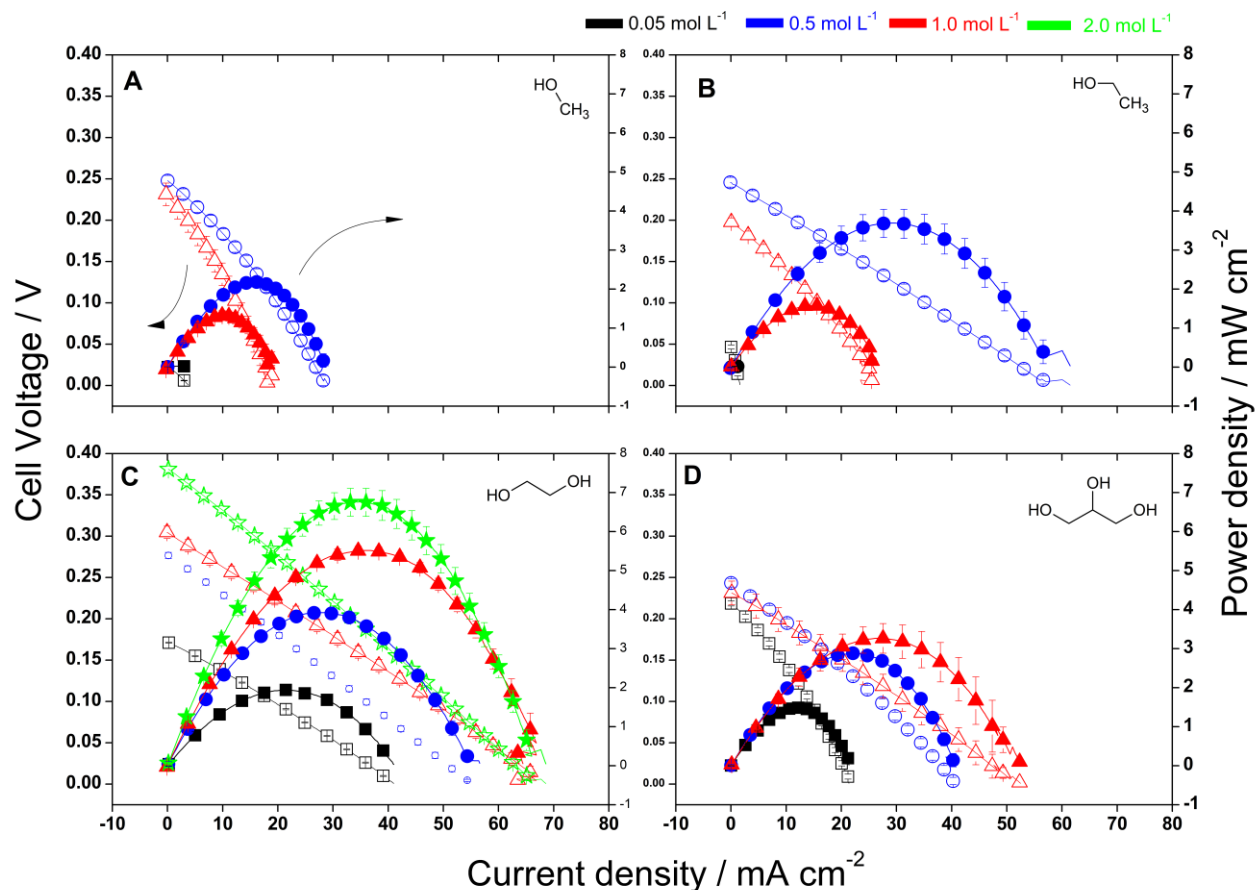
Figure 5. Polarization and power density curves for the paper-based microfluidic fuel cell fed by (A) methanol, (B) ethanol, (C) ethylene glycol, and (D) glycerol in 1 mol L⁻¹ KOH anolytes and by 0.5 mol L⁻¹ $Na_2S_2O_8$ in 1.0 mol L⁻¹ H_2SO_4 catholyte. Polarization curves were measured from open-circuit voltage to 0.001 V at 0.01 V s⁻¹. The different alcohol concentrations are shown in the figure. All measurements are in triplicate.

The PµFC fed by ethylene glycol displays the best performance, as shown in **Figure 5C**. PµFC fed by methanol and ethanol displays maximum power density at 0.5 mol L⁻¹, and lower performance for higher concentrations. On the hand, the overall performance increases with concentration from 0.05 to 1.0 mol L⁻¹ with ethylene glycol, thus we performed measurements with 1.5, 2.0, and 2.5 mol L⁻¹ to find the limits in terms of output power for this system. **Figure S7** shows all measurements.

The peak power density is 1.94 mW cm⁻² at 0.09 V when fed by 0.05 mol L⁻¹ ethylene glycol anolyte. The power density increases to 3.93 mW cm⁻² at 0.14 V fed by 0.5 mol L⁻¹ with 53.8 mA cm⁻² of maximum current density. By feeding the cell with 1.0 mol L⁻¹, the maximum power density reaches 5.52 mW cm⁻² at 0.15 V with 66.4 mA cm⁻² as the current density close to the short circuit (**Table 1**). The peak power density reaches 6.37 mW cm⁻² with 1.5 mol L⁻¹,

with 0.33 V of OCV, and 72.3 mA cm⁻² as maximum current density. This performance is higher than the state-of-the-art power density previously found by Chandra et al.[20] The best configuration appears when feeding the cell with 2.0 mol L⁻¹, revealing the benchmarking power density of 6.76 mW cm⁻² at 0.20 V. At least under our knowledge, this is the highest power density reported for an alcohol-fed PµFC, as shown in **Table 1**. Higher concentrations, such as 2.5 mol L⁻¹, saturate the system leading to a decrease in power density towards 4.8 mW cm⁻². This first developed ethylene glycol-fed PµFC displays remarkable output power.

Although the complete electrooxidation of ethylene glycol (eq. 3) implies less 2e⁻ harvested than for ethanol electrooxidation (eq. 2), ethylene glycol has two hydrated carbons, which facilitates the reaction. The different concentrations of ethylene glycol change the residence time of the

reactants deeply. The best performance at 2.0 mol L^{-1} appears at 3.75 10^{-3} cm s^{-1}, while it is 7.75 10^{-3} cm s^{-1} for 0.05 mol L^{-1}. Although 2.5 mol L^{-1} increases residence time (see flow rates in **Table S1**), the probable poisoning or saturation leads to a decrease in overall performance.

PµFCs fed by glycerol show improvement in performance from 0.05 to 1.00 mol L^{-1}, and further decrease for 1.50 mol L^{-1}, as shown in **Figure 5D**. The cell shows 1.49 mW cm^{-2} as the maximum power density at 0.12 V for 0.05 mol L^{-1}. When fed by 0.5 mol L^{-1} solution, the output power density increases to 2.89 mW cm^{-2} at 0.13 V with 39.3 mA cm^{-2} as the maximum current density. Feeding the cell with 1.0 mol L^{-1} glycerol in an alkaline solution delivers 3.27 mW cm^{-2} with 51.7 mA cm^{-2} (**Table 1**). Increasing concentration is deleterious. The use of 1.5 mol L^{-1} glycerol renders a high OCV of 0.30 V, but very limited electron transfer, leading to 2.18 mW cm^{-2} of peak power density. The residence time increases with the decrease in flow rate, thus the maximum power density is found in 1.0 mol L^{-1}, which is roughly half of that found for 0.05 mol L^{-1} (**Table S1**). Similar to the

features of the PµFC fed by ethylene glycol, high concentration leads to poisoning and saturation, being 1.0 mol L^{-1} as the limit. Half-cell measurements showed that the poisoning effect is more intense in high concentrations,[27] which was also reported for PDMS-based µFCs.[10] The three-hydrated carbons make the surface reaction very complex to understand,[6,11,25,33] but certainly improve electron harvest compared to methanol.

Most of the PµFCs fed by biomass-derived alcohols reported here are also higher than those reported in the literature, even considering other fuels and oxidants.[16] Under our knowledge, the systems that deliver higher power density than reported here are fed by other liquids, such as formic acid,[17] potassium formate in stacks,[18] zinc and vanadium,[34] and others detailed by Tanveer et al.[16] Moreover, the PµFC reported here may benefit further from an improved design, such as folding,[35] adding patterns to change the flow mechanism,[23] changing the size of electrodes, and flow configuration.[16]

Table 1. General parameters and performance comparison of the paper-based biomass microfluidic fuel cells. Fuels are methanol (MeOH), ethanol (EtOH), ethylene glycol (EgOH), and glycerol (GlOH).

	Fuel	Observation	Peak power potential / V	Peak power density / mW cm^{-2}	Maximum current density / mA cm^{-2}	OCV / V
This work	MeOH	0.05 mol L^{-1}	0.012	0.025	3.75	0.02
This work	MeOH	0.50 mol L^{-1}	0.14	2.18	28.6	0.25
This work	MeOH	1.00 mol L^{-1}	0.13	1.33	19.0	0.23
This work	EtOH	0.05 mol L^{-1}	0.027	0.023	1.63	0.05
This work	EtOH	0.50 mol L^{-1}	0.13	3.70	60.8	0.25
This work	EtOH	1.00 mol L^{-1}	0.11	1.57	25.6	0.20
This work	EgOH	0.05 mol L^{-1}	0.09	1.94	39.5	0.17
This work	EgOH	0.50 mol L^{-1}	0.14	3.93	53.8	0.28
This work	EgOH	1.00 mol L^{-1}	0.15	5.52	66.4	0.30
This work	EgOH	1.50 mol L^{-1}	0.18	6.37	72.3	0.33
This work	EgOH	2.00 mol L^{-1}	0.20	6.76	65.6	0.38
This work	EgOH	2.50 mol L^{-1}	0.17	4.8	50.9	0.35
This work	GlOH	0.05 mol L^{-1}	0.12	1.49	21.39	0.22
This work	GlOH	0.50 mol L^{-1}	0.13	2.89	39.3	0.24
This work	GlOH	1.00 mol L^{-1}	0.12	3.27	51.7	0.23
This work	GlOH	1.50 mol L^{-1}	0.16	2.18	24.8	0.30
Esquivel et al.[19]	MeOH	Pt cathode PtRu on Au/COP anode	-	4.4	47	0.55
Chandra et al.[20]	EtOH	MoO$_3$ electrodes; Gel membrane;	-	6.32	~13	~1.4
Rao et al.[21]	EtOH	MWCNTs	-	~0.073	~1.76	~0.25

Figure 6 reveals the limits in terms of the peak power density of the biomass-fed PµFC with different concentrations of alcohols. All graphs display a volcano-like behavior with their maxima. Cells fed by methanol and

ethanol show peaks at 0.05 mol L⁻¹. The peak power density is displaced to 1.0 mol L⁻¹ for cells fed by glycerol, suggesting that the anode tolerates a high concentration of this fuel. The difficulty in cleaving the two C-C bonds induces the formation of less CO compared to methanol (and probably ethanol), which is due to the partial glycerol electro-oxidation. The curve displays a peak at 2.0 mol L⁻¹ of ethylene glycol, suggesting an even higher tolerance to the excess of alcohol and improved fuel utilization in higher residence times. We hypothesize that the equilibrium between the number of C-C bonds and the oxidation state of the carbons might be the key to such performance. The presence of a C-C bond leads to less CO than a single-carbon fuel due to the increased partial oxidation, but oxidation is facilitated for the two hydrated carbons compared to hydrocarbons, which improves electron harvest with low CO poisoning.
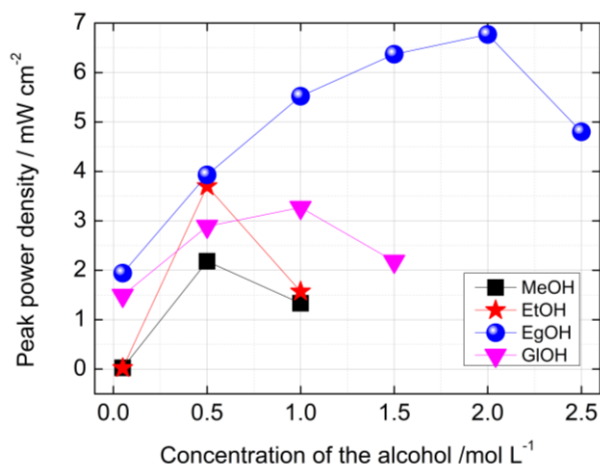
Figure 6. Peak power densities of the PµFC fed by different alcohols in different concentrations of anolytes.

In summary, whether needed, the PµFC displays similar output power density by interchanging the four fuels using 0.5 mol L⁻¹ (~2.2-3.9 mW cm⁻²) (**Figure 6**). This allows choosing the available fuel to deliver similar power, which may be demanded by portable devices that require an exact amount of energy. This analysis evidences that it is possible to improve performance by simply chemistry and engineering. For example, the output power of PµFCs fed by ethylene glycol is enhanced ~3.5 times only by adjusting the concentration of the fuel. Moreover, ethylene glycol is the most promising among these biomass-derived fuels, displaying the benchmark performance using a metal-free cathode.

4. **Conclusions**

This work demonstrated a paper battery based on colaminar microfluidic fuel cell configuration (PµFC) fed by biomass-derived fuels. Equipped with a Pt/C/CP anode and a metal-free CP cathode, the cell delivers high output power. The main strategy is to optimize each half-cell reaction independently in the membraneless cell. Namely, the PµFCs are fed by methanol, ethanol, ethylene glycol, or

glycerol in an alkaline medium for the anodic reaction, and by $N_2S_2O_8$ in an acidic medium for the cathodic reaction. The performance depends on the concentration and type of fuel, with consequences to the anode poisoning, residence time, and viscosity of the liquids.

Before operating the PµFC, we investigated the anodic half-cell measurements in porous Pt/C/CP, which show dependence on biomass-derived fuels. Methanol, ethanol, and glycerol show an increase in current density up to a maximum, and a followed drop, while the increase in ethylene glycol concentration increases current density up to a platô. Moreover, ethylene glycol electro-oxidation shows current densities more than 10 times higher than those for the other alcohols, suggesting improved kinetics. These results suggest that the structure of the alcohol plays a role besides concentration. The well-known CO intermediate, from small-chain alcohol oxidation, poisons the Pt surface, limiting the surface reaction. This effect is different for the different alcohols and counterbalances the faradic current delivered by the reaction. Therefore, the two hydrated carbon with only one bond of ethylene glycol makes this fuel the most powerful among the investigated ones.

The colaminar flow of the cellulose paper-based cells was investigated chemically and physically. We followed the cathodic, anodic, and interface regions by chemical mapping composition. The analysis reveals that each side is richer in its respective element from the electrolyte (anolyte and catholyte) and that the interface contains a proper mixture of both, chemically assuring the colaminar flow. Moreover, we investigated for the first time the flow rate (or velocity) based on recorded videos. The time to establish a stable colaminar flow for all cells is ~150-200 s, which coincides with the time to reach stable open circuit voltage. After this inflection point, the distance vs. time curves display approximately linear features. The linear fittings show that flow rates are similar regardless of concentration for methanol and ethanol but change deeply for more viscous fuels, such as ethylene glycol and glycerol. For instance, 2.0 mol L⁻¹ of ethylene glycol leads to half of the flow rate found with 0.05 mol L⁻¹. The decrease in velocity represents an increase in residence time, which may be beneficial for the anodic surface reaction.

The PµFCs equipped with Pt/C/CP anode and metal-free CP cathode were fed by the fuels in different concentrations in an alkaline medium as an anolyte and by $Na_2S_2O_4$ in an acidic medium as a catholyte. The peak power densities increase with concentration until their maxima and decrease after this limit. This volcano-like feature is different among the PµFCs fed by different fuels. Paper batteries fed by methanol and ethanol show their limits with 0.5 mol L⁻¹, while it is displaced to 1.0 mol L⁻¹ for glycerol and to 2.0 mol L⁻¹ for cells fed by ethylene glycol. Ethylene glycol show improved kinetics, as a result of the lower poisoning, and also shows lower residence time for 2.0 mol L⁻¹, which enhances performance. In higher concentrations, the poisoning and surface saturation become more relevant than the increase in residence time, and the performance is compromised. The limiting power densities of the cells are

composed of a balance among the poisoning of the anode, the residence time, and the viscosity of the liquids.

The biomass-derived fuel can be interchanged to feed the PµFCs to deliver ~2.2-3.9 mW cm⁻². Moreover, the cell fed by 2.0 mol L⁻¹ ethylene glycol using a metal-free cathode for $Na_2S_2O_8$ reduction delivers 6.76 mW cm⁻², which is the benchmark for a paper battery fed by alcohol. Here we show that the chemistry and engineering of the paper battery may be as important as producing new catalysts, and sometimes simple configuration changes lead to better performances than using time-consuming and complex new catalysts. We hope this work encourages researchers to explore theoretical and experimental configurations to boost output power, which might fasten the development of the field.

ASSOCIATED CONTENT

Supporting Information. Scanning microscopy images and energy-dispersive X-ray analysis of CP and Pt/C/CP. Photograph of the system. Half-cell measurements of the cathodic reaction. The calculation of the flow rates and the linear fittings. Polarization and power density curves.

AUTHOR INFORMATION

Corresponding Author

*caue.martins@ufms.br.

Author Contributions

The manuscript was written through the contributions of all authors. All authors have approved the final version of the manuscript.

ACKNOWLEDGMENT

REFERENCES

(1) Ibrahim, O. A.; Navarro-Segarra, M.; Sadeghi, P.; Sabaté, N.; Esquivel, J. P.; Kjeang, E. Microfluidics for Electrochemical Energy Conversion. *Chem. Rev.* **2022**. 7, 7236–7266. https://doi.org/10.1021/acs.chemrev.1c00499.

(2) Martins, C. A. Chapter 3 - Alcohol Fuel Cell on-a-Chip. In *Nanotechnology in Fuel Cells*; Song, H., Nguyen, T. A., Yasin, G., Eds.; Micro and Nano Technologies; Elsevier, **2022**; 41–76. https://doi.org/10.1016/B978-0-323-85727-7.00002-3.

(3) Gurrola, M. P.; Escalona-Villalpando, R. A.; Arjona, N.; Ledesma-García, J.; Arriaga, L. G. Microfluidic Fuel Cells. In *Encyclopedia of Electrochemistry*; John Wiley & Sons, Ltd, **2021**; 1–16. https://doi.org/10.1002/9783527610426.bard120075.

(4) Cohen, J. L.; Volpe, D. J.; Westly, D. A.; Pechenik, A.; Abruña, H. D. A Dual Electrolyte H2/O2 Planar Membraneless Microchannel Fuel Cell System with Open Circuit Potentials in Excess of 1.4 V. *Langmuir* **2005**, *21* (8), 3544–3550. https://doi.org/10.1021/la0479307.

(5) Kjeang, E.; Michel, R.; Harrington, D. A.; Djilali, N.; Sinton, D. A Microfluidic Fuel Cell with Flow-Through Porous Electrodes. *J. Am. Chem. Soc.* **2008**, *130* (12), 4000–4006. https://doi.org/10.1021/ja078248c.

(6) de Souza, M. B. C.; Guima, K.-E.; Fernández, P. S.; Martins, C. A. Glycerol Is Converted into Energy and Carbonyl Compounds in a 3D-Printed Microfluidic Fuel Cell: In Situ and In Operando Bi-Modified Pt Anodes. *ACS Appl. Mater. Interfaces* **2022**. 14 25457–25465. https://doi.org/10.1021/acsami.2c04313.

(7) Guima, K.-E.; L. Coelho, P.-H.; G. Trindade, M. A.; Alves Martins, C. 3D-Printed Glycerol Microfluidic Fuel Cell. *Lab on a Chip* **2020**, *20* (12), 2057–2061. https://doi.org/10.1039/D0LC00351D.

(8) Martins, C. A.; Pei, P.; Tellis, M.; Ibrahim, O. A.; Kjeang, E. Graphene-Oxide-Modified Metal-Free Cathodes for Glycerol/Bleach Microfluidic Fuel Cells. *ACS Appl. Nano Mater.* **2020**. 3 (8) 8286–8293. https://doi.org/10.1021/acsanm.0c01722.

(9) Martins, C. A.; Ibrahim, O. A.; Pei, P.; Kjeang, E. In Situ Decoration of Metallic Catalysts in Flow-through Electrodes: Application of Fe/Pt/C for Glycerol Oxidation in a Microfluidic Fuel Cell. *Electrochimica Acta* **2019**, *305*, 47–55. https://doi.org/10.1016/j.electacta.2019.03.018.

(10) Martins, C. A.; Ibrahim, O. A.; Pei, P.; Kjeang, E. Towards a Fuel-Flexible Direct Alcohol Microfluidic Fuel Cell with Flow-through Porous Electrodes: Assessment of Methanol, Ethylene Glycol and Glycerol Fuels. *Electrochimica Acta* **2018**, *271*, 537–543. https://doi.org/10.1016/j.electacta.2018.03.197.

(11) Martins, C. A.; Giz, M. J.; Camara, G. A. Generation of Carbon Dioxide from Glycerol: Evidences of Massive Production on Polycrystalline Platinum. *Electrochimica Acta* **2011**, *56* (12), 4549–4553. https://doi.org/10.1016/j.electacta.2011.02.076.

(12) Martins, C. A.; Fernández, P. S.; Troiani, H. E.; Martins, M. E.; Camara, G. A. Ethanol vs. Glycerol: Understanding the Lack of Correlation between the Oxidation Currents and the Production of CO2 on Pt Nanoparticles. *Journal of Electroanalytical Chemistry* **2014**, *717–718*, 231–236. https://doi.org/10.1016/j.jelechem.2014.01.027.

(13) Fernández, P. S.; Martins, M. E.; Martins, C. A.; Camara, G. A. The Electro-Oxidation of Isotopically Labeled Glycerol on Platinum: New Information on C–C Bond Cleavage and CO2 Production. *Electrochemistry Communications* **2012**, *15* (1), 14–17. https://doi.org/10.1016/j.elecom.2011.11.013.

(14) A. Martins, C.; A. Ibrahim, O.; Pei, P.; Kjeang, E. "Bleaching" Glycerol in a Microfluidic Fuel Cell to Produce High Power Density at Minimal Cost. *Chemical Communications* **2018**, *54* (2), 192–195. https://doi.org/10.1039/C7CC08190A.

(15) *Microfluidic Fuel Cells and Batteries | Erik Kjeang | Springer*; 2017.

(16) Tanveer, M.; Ambreen, T.; Khan, H.; Man Kim, G.; Woo Park, C. Paper-Based Microfluidic Fuel Cells and Their Applications: A Prospective Review. *Energy Conversion and Management* **2022**, *264*, 115732. https://doi.org/10.1016/j.enconman.2022.115732.

(17) Arun, R. K.; Halder, S.; Chanda, N.; Chakraborty, S. A Paper Based Self-Pumping and Self-Breathing Fuel Cell Using Pencil Stroked Graphite Electrodes. *Lab Chip* **2014**, *14* (10), 1661–1664. https://doi.org/10.1039/C4LC00029C.

(18) Li, L.; He, Y.; Xu, Q.; Liu, T.; Bei, S.; Zheng, K.; Yang, J.; Wang, H.; Leung, M. K. H. A Paper-Based Self-Pumping Microfluidic Fuel Cell Stack with a Novel Vertical

Structure. *International Journal of Energy Research.* **2022**, *46* 8389-8397. https://doi.org/10.1002/er.7742.

(19) Esquivel, J. P.; Campo, F. J. D.; Fuente, J. L. G. de la; Rojas, S.; Sabaté, N. Microfluidic Fuel Cells on Paper: Meeting the Power Needs of next Generation Lateral Flow Devices. *Energy Environ. Sci.* **2014**, *7* (5), 1744–1749. https://doi.org/10.1039/C3EE44044C.

(20) Chandra, S.; Lal, S.; Janardhanan, V. M.; Sahu, K. C.; Deepa, M. Ethanol Based Fuel Cell on Paper Support. *Journal of Power Sources* **2018**, *396*, 725–733. https://doi.org/10.1016/j.jpowsour.2018.06.068.

(21) Rao, L. T.; Dubey, S. K.; Javed, A.; Goel, S. Stacked Microfluidic Paper Ethanol Fuel Cell with a Variety of Rapidly Prototyped Electrodes: Optimization and Performance Investigation. *Energy Technology.* **2022**, *10*, 2200073. https://doi.org/10.1002/ente.202200073.

(22) Martins, C. A.; Fernández, P. S.; Camara, G. A. Alternative Uses for Biodiesel Byproduct: Glycerol as Source of Energy and High Valuable Chemicals. In *Increased Biodiesel Efficiency*; Green Energy and Technology; Springer, Cham, **2018**; pp 159–186. https://doi.org/10.1007/978-3-319-73552-8_7.

(23) Anushka; Bandopadhyay, A.; Das, P. K. Paper Based Microfluidic Devices: A Review of Fabrication Techniques and Applications. *Eur. Phys. J. Spec. Top.* **2022**. https://doi.org/10.1140/epjs/s11734-022-00727-y.

(24) Goulet, M.-A.; Skyllas-Kazacos, M.; Kjeang, E. The Importance of Wetting in Carbon Paper Electrodes for Vanadium Redox Reactions. *Carbon* **2016**, *101*, 390–398. https://doi.org/10.1016/j.carbon.2016.02.011.

(25) Fernández, P. S.; Martins, C. A.; Angelucci, C. A.; Gomes, J. F.; Camara, G. A.; Martins, M. E.; Tremiliosi-Filho, G. Evidence for Independent Glycerol Electrooxidation Behavior on Different Ordered Domains of Polycrystalline Platinum. *CHEMELECTROCHEM* **2015**, *2* (2), 263–268. https://doi.org/10.1002/celc.201402291.

(26) Fernández, P. S.; Martins, C. A.; Martins, M. E.; Camara, G. A. Electrooxidation of Glycerol on Platinum Nanoparticles: Deciphering How the Position of Each Carbon Affects the Oxidation Pathways. *Electrochimica Acta* **2013**, *112*, 686–691. https://doi.org/10.1016/j.electacta.2013.09.032.

(27) Gomes, J. F.; Martins, C. A.; Giz, M. J.; Tremiliosi-Filho, G.; Camara, G. A. Insights into the Adsorption and Electro-Oxidation of Glycerol: Self-Inhibition and Concentration Effects. *Journal of Catalysis* **2013**, *301*, 154–161. https://doi.org/10.1016/j.jcat.2013.02.007.

(28) Teles, R.; Arenillas, A.; Silva, G. C. da; Fernández, P. S.; Cardoso, E. S. F.; Maia, G.; Martins, C. A. Understanding the Influence of the Biomass-Derived Alcohols on the Activity and Stability of Pt Nanoparticles Supported on Graphene Nanoribbons. *Electrocatalysis* **2017**, 1–13. https://doi.org/10.1007/s12678-016-0349-3.

(29) Ouyang, T.; Lu, J.; Xu, P.; Hu, X.; Chen, J. Mechanism Study and Evaluation of High Efficiency Paper-Based Microfluidic Fuel Cell Coupled with Capillary Force. *Journal of Power Sources* **2022**, *520*, 230807. https://doi.org/10.1016/j.jpowsour.2021.230807.

(30) Whitaker, S. Flow in Porous Media I: A Theoretical Derivation of Darcy's Law. *Transp Porous Med* **1986**, *1* (1), 3–25. https://doi.org/10.1007/BF01036523.

(31) Abbasiasl, T.; Mirlou, F.; Istif, E.; Koydemir, H. C.; Beker, L. A Wearable Paper-Integrated Microfluidic Device for Sequential Analysis of Sweat Based on Capillary Action. *Sensors & Diagnostics* **2022**, *1* (4), 775–786. https://doi.org/10.1039/D2SD00032F.

(32) Giz, M. J.; Camara, G. A. The Ethanol Electrooxidation Reaction at Pt (1 1 1): The Effect of Ethanol Concentration. *Journal of Electroanalytical Chemistry* **2009**, *625* (2), 117–122. https://doi.org/10.1016/j.jelechem.2008.10.017.

(33) Fernández, P. S.; Fernandes Gomes, J.; Angelucci, C. A.; Tereshchuk, P.; Martins, C. A.; Camara, G. A.; Martins, M. E.; Da Silva, J. L. F.; Tremiliosi-Filho, G. Establishing a Link between Well-Ordered Pt(100) Surfaces and Real Systems: How Do Random Superficial Defects Influence the Electro-Oxidation of Glycerol? *ACS Catal.* **2015**, *5* (7), 4227–4236. https://doi.org/10.1021/acscatal.5b00451.

(34) Pasala, V.; Ramanujam, K. Paper-Based Disposable Zinc-Vanadium Fuel Cell for Micropower Applications. *ChemistrySelect* **2019**, *4* (29), 8398–8403. https://doi.org/10.1002/slct.201802624.

(35) Juqu, T.; Willenberg, S. C.; Pokpas, K.; Ross, N. Advances in Paper-Based Battery Research for Biodegradable Energy Storage. *Advanced Sensor and Energy Materials* **2022**, 100037. https://doi.org/10.1016/j.asems.2022.100037.